Inorg. Chem. **2005**, *44*, 3031–3045

Reduction Pathway of End-On Terminally Coordinated Dinitrogen. V. N–N Bond Cleavage in Mo/W Hydrazidium Complexes with Diphosphine Coligands. Comparison with Triamidoamine Systems

Klaus Mersmann,[†] Kay H. Horn,[†] Natascha Böres,[†] Nicolai Lehnert,[†] Felix Studt,[†] Florian Paulat,[†] Gerhard Peters,[†] Ivana Ivanovic-Burmazovic,[‡] Rudi van Eldik,*[,‡] and Felix Tuczek*[,†]

Institut für Anorganische Chemie, Christian-Albrechts-Universität Kiel, Otto Hahn Platz 6/7, 24098 Kiel, Germany, and Institut für Anorganische Chemie, Friedrich-Alexander Universität Erlangen-Nürnberg, Egerlandstrasse 1, 91058 Erlangen, Germany

Received September 22, 2004

N–N cleavage of the dialkylhydrazido complex $[W(dppe)_2(NNC_5H_{10})]$ ($\mathbf{B}^W$) upon treatment with acid, leading to the nitrido/imido complex and piperidine, is investigated experimentally and theoretically. In acetonitrile and at room temperature, $\mathbf{B}^W$ reacts orders of magnitude more rapidly with $HNEt_3BPh_4$ than its Mo analogue, $[Mo(dppe)_2(NNC_5H_{10})]$ ($\mathbf{B}^{Mo}$). A stopped-flow experiment performed for the reaction of $\mathbf{B}^W$ with $HNEt_3BPh_4$ in propionitrile at −70 °C indicates that protonation of $\mathbf{B}^W$ is completed within the dead time of the stopped-flow apparatus, leading to the primary protonated intermediate $\mathbf{B}^WH^+$. Propionitrile coordination to this species proceeds with a rate constant $k_{obs(1)}$ of 1.5 ± 0.4 s^{-1}, generating intermediate RCN–$\mathbf{B}^WH^+$ (R = Et) that rapidly adds a further proton at N_β and then mediates N–N bond splitting in a slower reaction ($k_{obs(2)} = 0.35 \pm 0.08$ s^{-1}, 6 equiv of acid). $k_{obs(1)}$ and $k_{obs(2)}$ are found to be independent of the acid concentration. The experimentally observed reactivities of $\mathbf{B}^{Mo}$ or $\mathbf{B}^W$ with acids in nitrile solvents are reproduced by DFT calculations. In particular, geometry optimization of models of solvent-coordinated, N_β-protonated intermediates is found to lead spontaneously to separation into the nitrido/imido complexes and piperidine/piperidinium, corresponding to activationless heterolytic N–N bond cleavage processes. Moreover, DFT indicates a spontaneous cleavage of nonsolvated $\mathbf{B}^W$ protonated at N_β. In the second part of this article, a theoretical analysis of the N–N cleavage reaction in the Mo(III) triamidoamine complex $[HIPTN_3N]Mo(N_2)$ is presented (HIPTN$_3$N = hexaisopropylterphenyltriamidoamine). To this end, DFT calculations of the $Mo^{III}N_2$ triamidoamine complex and its protonated and reduced derivatives are performed. Calculated structural and spectroscopic parameters are compared to available experimental data. N–N cleavage most likely proceeds by one-electron reduction of the Mo(V) hydrazidium intermediate $[HIPTN_3N]Mo(NNH_3)^+$, which is predicted to have an extremely elongated N–N bond. From an electronic-structure point of view, this reaction is analogous to that of Mo/W hydrazidium complexes with diphos coligands. The general implications of these results with respect to synthetic N_2 fixation are discussed.

I. Introduction

Because of the triple bond present in N_2, N−N cleavage of this molecule is highly endothermic in the gas phase. The corresponding bond dissociation enthalpy (225 kcal mol^{-1})[1] can be dramatically lowered if dinitrogen is coordinated to transition-metal centers. In some dinitrogen complexes, N−N bond splitting is even possible under ambient conditions. Thus, spontaneous N−N cleavage has been detected for dinitrogen coordinated in an end-on or side-on bridging geometry to two transition-metal centers.[2] Alternatively, N−N cleavage is facilitated if the bond order has been reduced through protonation and/or alkylation.[3,4] This reaction mode also applies to the reduction pathway of N_2 coordinated end-on terminally to mononuclear transition-metal complexes.[5] Importantly, the latter pathway is considered to apply to the reduction and protonation of N_2 in

* To whom correspondence should be addressed. E-mail: ftuczek@ac.uni-kiel.de (F.T.), vaneldik@chemie.uni-erlangen.de (R.v.E.).
[†] Christian-Albrechts-Universität Kiel.
[‡] Friedrich-Alexander Universität Erlangen-Nürnberg.

(1) Cotton, F. A.; Murillo, C. A.; Bochmann, M.; Wilkinson G. *Advanced Inorganic Chemistry*, 6th ed.; John Wiley & Sons: New York, 1999.

10.1021/ic048674o CCC: $30.25
Published on Web 03/29/2005

the enzyme nitrogenase, which catalyzes the biological process of nitrogen fixation.[6]

If N_2 is coordinated end-on terminally to Mo/W complexes with diphosphine coligands, N−N cleavage requires two-electron reduction at the level of NNH_2 intermediates.[7] For practical reasons, these reactions have been studied using alkylated derivatives.[3] Thus, two-electron reduction of the Mo(IV) dialkylhydrazido(2−) complex $[MoBr(NNC_5H_{10})(dppe)_2]Br$ (compound $\mathbf{A}^{Mo}$) with BuLi or electrochemically has been found to generate under reductive elimination of the trans bromo ligand the five-coordinate, two-electron-reduced intermediate $[Mo(NNC_5H_{10})(dppe)_2]$ (compound $\mathbf{B}^{Mo}$), protonation of which with HBr in THF leads to formation of HNC_5H_{10} (piperidine) and the imido complex $[MoBr(NH)(dppe)_2]Br$ under cleavage of the N−N bond. The kinetics of this process has been studied in detail by Henderson et al. using nitrile solvents RCN and the weak acid $HNEt_3BPh_4$ (R = Me, Et, Ph).[8] Under these conditions, the observed rate constant of the overall splitting reaction, k_{obs}, is greatly decreased, and the nitrido and imido compounds $[(RCN)Mo(N)(dppe)_2]BPh_4$ and $[(RCN)Mo(NH)(dppe)_2](BPh_4)_2$, respectively, are obtained as final products (Scheme 1).

On the basis of the kinetic data, the alkylhydrazidium species $[Mo(NNHC_5H_{10})(dppe)_2]^+$ ($\mathbf{B}^{Mo}H^+$) has been postulated as the primary product resulting from protonation of $\mathbf{B}^{Mo}$. In nitriles, addition of a solvent molecule RCN to $\mathbf{B}^{Mo}H^+$ then was hypothesized to generate the six-coordinate intermediate $[(RCN)Mo(NNHC_5H_{10})(dppe)_2]^+$ ($RCN-\mathbf{B}^{Mo}H^+$), which subsequently rearranges to a bent alkylhydrazidium structure (R = Me, Et, Ph). This species either directly decays to the nitrido complex and piperidine with a rate constant k_4 or adds another proton at N_α to generate a doubly protonated species that subsequently undergoes N−N splitting with a rate constant k_5. The direct (k_4) and proton-assisted (k_5) decay channels of the primary intermediate $\mathbf{B}^{Mo}H^+$ both contribute to a N−N cleavage rate constant k_{obs} on the order of 1−60 s^{-1}, much smaller than that found for the reaction of compound $\mathbf{B}^{Mo}$ with HBr in THF ($k_{obs} > 300\ s^{-1}$).

Scheme 1. Mechanism of Reaction between $\mathbf{B}^{Mo}$ and Acid (Henderson et al.[8])

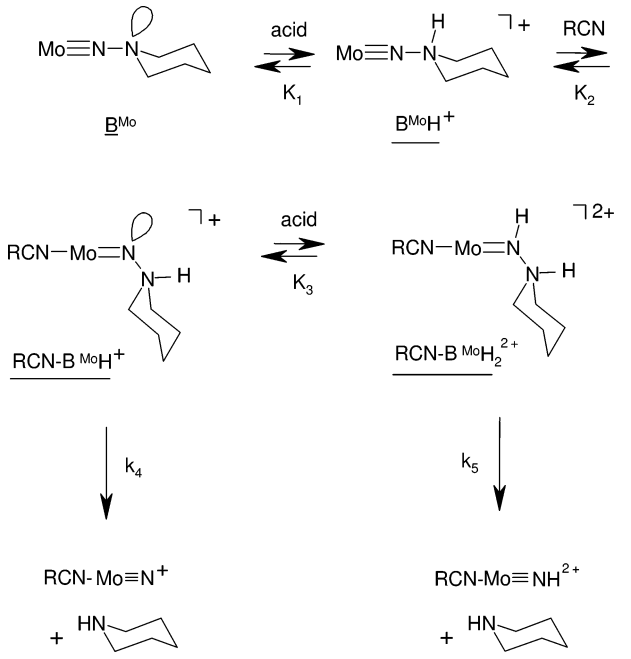

In the accompanying article,[9] compounds $\mathbf{A}^{Mo}$ and $\mathbf{B}^{Mo}$ and their tungsten counterparts $\mathbf{A}^{W}$ and $\mathbf{B}^{W}$ are characterized by X-ray structure analysis, spectroscopy, and DFT calculations on the model complex $[Mo(NNC_5H_{10})(PH_2C_2H_4PH_2)_2]$ ($\tilde{\mathbf{B}}$).[9] On the basis of these results, the N−N splitting of compound $\mathbf{B}^{W}$ is investigated spectroscopically and theoretically in the present study with the goal of elucidating the contributions of electronic structure to this process. Particular attention is thereby directed toward correlating the results of the theoretical treatment to the available kinetic and spectroscopic data and understanding the influence of the solvent and the acid on the mechanism of this reaction. To this end, the N−N cleavage process of $\mathbf{B}^{W}$ is monitored at various temperatures in different solvents (THF, acetonitrile, propionitrile, benzonitrile), employing $HNEt_3BPh_4$ and $HLutBPh_4$ as acids (Lut = 2,6-lutidine). Importantly, the reaction of $\mathbf{B}^{W}$ with $HNEt_3BPh_4$ in acetonitrile at room temperature is found to be much faster than the corresponding reaction of $\mathbf{B}^{Mo}$. A stopped-flow experiment and corresponding kinetic analysis are therefore performed for the protonation of $\mathbf{B}^{W}$ with $HNEt_3BPh_4$ in propionitrile at −70 °C. The two-electron-reduced compounds $\mathbf{B}^{Mo}$ and $\mathbf{B}^{W}$ contain three potentially Lewis-basic centers, i.e., N_α, N_β, and the metal. DFT calculations are employed to obtain information on the protonation processes at these different sites and to understand the reactivities of the corresponding protonated intermediates.

(2) (a) Laplaza, C. E.; Johnson, A. R.; Cummins, C. C. *J. Am. Chem. Soc.* **1996**, *118*, 709 and references therein. (b) Clentsmith, G. K. B.; Bates, V. M.; Hitchcock, P. B.; Cloke, F. G. N. *J. Am. Chem. Soc.* **1996**, *118*, 709. (c) Caselli, A.; Solari, E.; Scopelliti, R.; Floriani, C.; Re, N.; Rizzoli, C.; Chiesi-Villa, A. *J. Am. Chem. Soc.* **2000**, *122*, 709. (d) Fryzuk, M. D.; Kozak, C. M.; Bowdridge, M. R.; Patrick, B. O.; Rettig, S. J. *J. Am. Chem. Soc.* **2002**, *124*, 8389. (e) Fryzuk, M. D.; MacKay, B. A.; Johnson, S. A.; Patrick, B. O. *Angew. Chem., Int. Ed.* **2002**, *41*, 3709. (f) Fryzuk, M. D.; MacKay, B. A.; Patrick, B. O. *J. Am. Chem. Soc.* **2003**, *125*, 3234.

(3) (a) Pickett, C. J.; Leigh, G. J. *J. Chem. Soc., Dalton* **1981**, 1033. (b) Hussain, W.; Leigh, G. J.; Pickett, C. J. *J. Chem. Soc., Chem. Commun.* **1982**, 747.

(4) (a) Fryzuk, M. D.; Love, J. B.; Rettig, S. J.; Young, V. G. *Science* **1997**, *275*, 1445. (b) Pool, J. A.; Lobkovski, E.; Chirik, P. J. *Nature* **2004**, *427*, 527. (c) Smith, J. M.; Lachicotte, R. J.; Holland, P. L. *J. Am. Chem. Soc.* **2003**, *125*, 15752. (d) Le Grand, N.; Muir, K. W.; Pétillon, F. Y.; Pickett, C. J.; Schollhammer, P.; Talarmin, J. *Chem. Eur. J.* **2002**, *8*, 3115 and references therein. (e) Ishino, H.; Tokunaga, Sh.; Seino, H.; Ishii, Y.; Hidai, M. *Inorg. Chem.* **1999**, *38*, 2489. (f) Schrock, R. R.; Glassman, T. E.; Vale, M. G.; Kol, M. *J. Am. Chem. Soc.* **1993**, *115*, 1760 and references therein.

(5) (a) MacKay, B. A.; Fryzuk, M. D. *Chem. Rev.* **2004**, *104*, 385. (b) Fryzuk, M. D.; Johnson, S. A. *Coord. Chem. Rev.* **2000**, *200−202*, 379. (c) Hidai, M. *Coord. Chem. Rev.* **1999**, *185−186*, 99. (d) Hidai, M.; Mizobe, Y. *Chem. Rev.* **1995**, *95*, 1115.

(6) Thorneley, R. N. F.; Lowe, D. J. In *Molybdenum Enzymes*; Spiro, T. G., Ed.; Wiley-Interscience: New York, 1985.

(7) Chatt, J.; Pearman, A. J.; Richards, R. L. *J. Chem. Soc., Dalton Trans.* **1977**, 1852.

(8) Henderson, R. A.; Leigh, G. J.; Pickett, C. J. *J. Chem. Soc., Dalton Trans.* **1989**, 425.

(9) Horn, K. H.; Böres, N.; Lehnert, N.; Mersmann, K.; Näther, C.; Peters, G.; Tuczek, F. **2005**, *44*, 3016−3030.

Chart 1. [$HIPTN_3N$]MoN_2 Complex

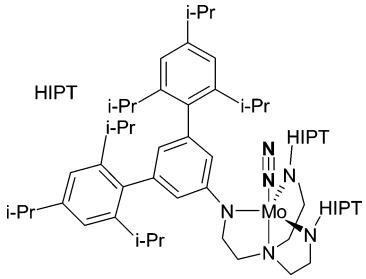

Whereas the protolytic N−N cleavage process of the alkylated compounds $\mathbf{B}^{Mo}$ and $\mathbf{B}^{W}$ provides considerable insight into the mechanistic features of this elementary reaction, the analogous step in the conversion of N_2 to NH_3 at Mo/W complexes with diphosphine ligands is complicated by cross reactions between NNH_2 species and their two-electron-reduced derivatives according to the simplified reaction

$$Mo^{IV}(NNH_2)^{2+} + Mo^{II}(NNH_2) \rightarrow Mo^{0}(N_2) + Mo^{IV}(NH)^{2+} + NH_3 \quad (1)$$

(where Mo = Mo(diphos)$_2$).[10] These problems have been overcome by using a Mo(III) complex with the novel triamidoamine ligand $[HIPTN_3N]^{3-}$ (hexaisopropylterphenyltriamidoamine), which provides a sterically shielded site for the conversion of N_2 to ammonia (Chart 1).[11] Insight into details of this process was obtained from the characterization of a number of intermediates. Specifically, protonation of the dinitrogen complex [$HIPTN_3N$]Mo(N_2) (**1**) was found to lead to the NNH and NNH_2 complexes [$HIPTN_3N$]Mo(NNH) (**1-H**) and [$HIPTN_3N$]Mo$(NNH_2)^+$ (**2**), which could be isolated and characterized.[11a,b] N−N cleavage of **2** was hypothesized to proceed via the further reduced and protonated intermediates [$HIPTN_3N$]Mo(NNH_2) (**3**) and [$HIPTN_3N$]Mo$(NNH_3)^+$ (**5**), generating NH_3 and the nitrido complex [$HIPTN_3N$]MoN (**6**), which could be isolated and characterized as well. By protonation and reduction of **6**, the Mo(IV) ammine complex [$HIPTN_3N$]Mo$(NH_3)^+$ is formed, which, upon one-electron reduction, is able to rebind N_2 under release of NH_3, closing the reactive cycle. Importantly, the catalytic conversion of N_2 to NH_3 has been demonstrated for this system, achieving six turnovers with a yield of 65%. This represents a significant improvement over the Mo/W diphosphine systems for which a conversion of N_2 to NH_3 in three cycles could be achieved, however, with a total yield of only 0.75 NH_3 per metal complex.[10]

As two paradigms are thus available for the cyclic conversion of N_2 to NH_3, it is of significant interest to compare the reactive properties of these two systems from an electronic structure point of view, particularly with respect to the question of how N−N cleavage is mediated. To this end, DFT calculations on models **I** and **II** of the N_2 complex [$HIPTN_3N$]Mo(N_2) (**1**) and its protonated/reduced derivative [$HIPTN_3N$]Mo$(NNH_2)^+$ (**2**) are presented here; Scheme 2 shows the corresponding calculated structures. For investigation of the subsequent N−N splitting, model **II** is first reduced by one electron, generating model **III** of neutral NNH_2 species [$HIPTN_3N$]Mo(NNH_2) (**3**). Then, one proton is added to **III**, generating model **V** of the postulated hydrazidium intermediate [$HIPTN_3N$]Mo$(NNH_3)^+$ (**5**), which cleaves the N−N bond upon further one-electron reduction (Scheme 2). Alternatively, addition of one electron to **III** is considered, generating model **IV** of the negatively charged hydrazido(2−) intermediate [$HIPTN_3N$]Mo$(NNH_2)^-$ (**4**), which cleaves the N−N bond upon further protonation. These reactions are compared to the analogous protolytic N−N splitting reactions of compounds $\mathbf{B}^{Mo}$ and $\mathbf{B}^{W}$ (vide supra). Moreover, the electronic structures of the various Mo triamidoamine N_2, NNH_2, and NNH_3 species **I**−**V** are

Scheme 2. Possible Mechanisms of N−N Cleavage at a [$HIPTN_3N$]Mo Center

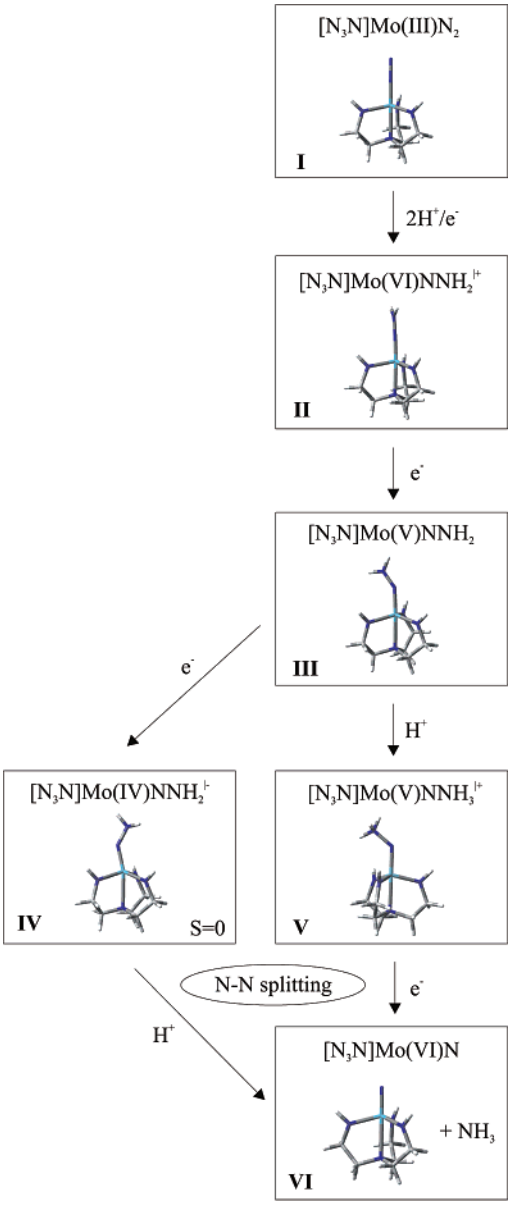

(10) Pickett, C. J.; Talarmin, J. *Nature (London)* **1985**, *317*, 652.
(11) (a) Yandulov, D. V.; Schrock, R. R. *J. Am. Chem. Soc.* **2002**, *124*, 6252. (b)Yandulov, D. V.; Schrock, R. R. *Science* **2003**, *301*, 76. (c) Yandulov, D. V.; Schrock, R. R.; Rheingold, A. L.; Ceccarelli, C.; Davis, W. M. *Inorg. Chem.* **2003**, *42*, 796. (d) Ritleng, V.; Yandulov, D. V.; Weare, W. W.; Schrock, R. R.; Hock, A. S.; Davis W. M. *J. Am. Chem. Soc.* **2004**, *126* (19), 6150.

determined. Metal−N and N−N distances as well as metal−N and N−N stretching frequencies are calculated, and theoretical predictions are compared to the available experimental data. The effects of the coligands and the d-electron configurations on the activation of the N_2 and NNH_x ligands are evaluated on the basis of electronic charges on the N_2 and NNH_x ligands. The theoretical results are correlated to the observed reactivities, and the implications on the transition-metal-mediated conversion of N_2 to NH_3 are discussed.

II. Experimental and Computational Procedures

Sample Preparation. $[W(NNC_5H_{10})(dppe)_2]$ (compound $\mathbf{B}^W$) was prepared as described in the accompanying article.[9] The ^{15}N-labeled compound was synthesized from the corresponding isotope-labeled dinitrogen complex $[W(^{15}N)_2(dppe)_2]$. All sample preparations were performed under a nitrogen or argon atmosphere using Schlenk techniques. All solvents were dried under argon. 2,6-Lutidine was purchased from Lancaster. Lutidine·$HBPh_4$ was synthesized from a metathesis reaction between lutidine·HCl and $NaBPh_4$ according to the method described in ref 12.

NMR Spectroscopy. ^{15}N NMR spectra were recorded on a Bruker Avance 400 Pulse Fourier transform spectrometer operating at a ^1H frequency of 400.13 MHz using a 5-mm inverse triple-resonance probe head. The reference as a substitutive standard was neat CH_3NO_2, $\delta(^{15}N) = 0$ ppm.

Stopped-Flow Measurements. Low-temperature kinetic data were obtained by recording time-resolved UV/vis spectra using a modified Bio-Logic stopped-flow module μSFM-20 instrument combined with cryo-stopped-flow accessory (Huber CC90 cryostat) and equipped with a J & M TIDAS high-speed diode array spectrometer with combined deuterium and tungsten lamp (200−1015 nm bandwidth). Isolast O-rings were used for all sealing purposes. Concentration-dependent measurements were performed by mixing different concentrations of $[HNEt_3]^+$ with at least 6 times lower concentrations of complex ([complex] = 0.053 mM) in a 1:1 volume ratio and also by using the same acid solution ($[[HNEt_3]^+]$ = 3.2 mM) and applying the option of a variable mixing volume ratio. During the measurements, nitrogen was flashed through the system. Data were analyzed using the integrated Bio-Kine software version 4.23 and also the Specfit/32 program.

DFT Calculations. Spin-restricted DFT calculations were performed for the model complex $[Mo(NNC_5H_{10})(PH_2C_2H_4PH_2)_2]$ ($\tilde{\mathbf{B}}$) and its solvent-coordinated and/or protonated derivatives using Becke's three-parameter hybrid functional with the correlation functional of Lee, Yang, and Parr (B3LYP).[13] The LANL2DZ basis set was used for the calculations. It applies the Dunning/Huzinaga full double-ζ (D95)[14] basis functions on the first row atoms and the Los Alamos effective core potentials plus DZ functions on all other atoms.[15] All computational procedures are used as they are implemented in the Gaussian 98 package.[16] Wave functions are plotted with the visualization program GaussView. Judging from the fact that the geometric and spectroscopic properties of $\mathbf{B}^W$ are well reproduced by $\tilde{\mathbf{B}}$, we refrained from carrying out parallel calculations on a W model system. Spin-restricted DFT calculations (B3LYP/LANL2DZ) were performed for the singlet ground state of model complexes $[N_3N]Mo^{VI}NNH_2^+$ (**II**) and $[N_3N]Mo^{IV}NNH_2^-$ (**IV**). In the case of model complexes $[N_3N]Mo^{III}N_2$ (**I**), $[N_3N]Mo^{V}NNH_2$ (**III**), $[N_3N]Mo^{IV}NNH_2^-$ (**IV**), and $[N_3N]Mo^{V}NNH_3^+$ (**V**), corresponding spin-unrestricted DFT calculations were performed for the doublet (**I**, **III**, **V**) and triplet (**IV**) states.

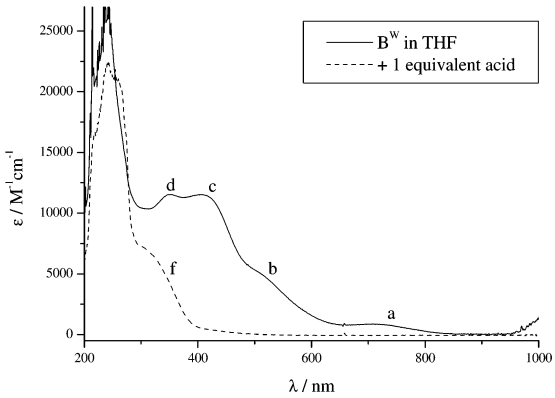

Figure 1. UV/vis spectrum of $\mathbf{B}^W$ and of protonation products in THF.

III. Results and Analysis

A. Protolytic N−N Cleavage of the W(dppe)$_2$ Dialkylhydrazido Complex $\mathbf{B}^W$. 1. Protonation of $\mathbf{B}^W$ with HLutBPh$_4$ in THF. The UV/vis absorption spectrum of $\mathbf{B}^W$ in THF is presented in Figure 1. Above 300 nm, it exhibits four bands at 720, 520, 412, and 350 nm that are denoted a−d. Upon protonation of $\mathbf{B}^W$ in THF at room temperature with 1 equiv of 2,6-lutidine·$HBPh_4$ (HLutBPh$_4$), bands a−d disappear within about 15 min, leaving a final spectrum (f) with an absorption feature at 320 nm.[17] Quantitative formation of piperidine in this reaction was demonstrated by GC. The 320-nm band in spectrum f is therefore associated with the nitrido complex $[W(dppe)_2(N)]^+$.

2. Protonation of $\mathbf{B}^W$ with HNEt$_3$BPh$_4$ in Propionitrile. To study the protolytic N−N cleavage of $\mathbf{B}^W$ in coordinating solvents, various nitriles were employed. Reaction of $\mathbf{B}^W$ with $HNEt_3BPh_4$ in acetonitrile was so fast that its kinetics could not be monitored, even with the stopped-flow technique at −35 °C. This indicates that the reaction of $\mathbf{B}^W$ with $HNEt_3BPh_4$ in this solvent is much faster than the corresponding reaction of $\mathbf{B}^{Mo}$, for which a stopped-flow study at room temperature has been performed.[8] Therefore, the reaction of $\mathbf{B}^W$ was investigated in propionitrile at −70 °C. UV/vis absorption spectra of $\mathbf{B}^W$ before and after protonation (Figure S1) are very similar to the corresponding spectra in THF

(12) Malinak, S. M.; Simeonov, A. M.; Mosier, P. E.; McKenna, C. E.; Coucouvanis, D. *J. Am. Chem. Soc*. **1997**, *119*, 1662.
(13) Becke, A. D. *J. Chem. Phys.* **1993**, *98*, 5648.
(14) Dunning, T. H., Jr.; Hay, P. J. In *Modern Theoretical Chemistry*; Schaefer, H. F., III, Ed.; Plenun: New York, 1976.
(15) (a) Hay, P. J.; Wadt, W. R. *J. Chem. Phys.* **1985**, *82*, 270 and 299. (b) Wadt, W. R.; Hay, P. J. *J. Chem. Phys.* **1985**, *82*, 284.
(16) Frisch, M. J.; Trucks, G. W.; Schlegel, H. B.; Scuseria, G. E.; Robb, M. A.; Cheeseman, J. R.; Zakrzewski, V. G.; Montgomery, J. A., Jr.; Stratmann, R. E.; Burant, J. C.; Dapprich, S.; Millam, J. M.; Daniels, A. D.; Kudin, K. N.; Strain, M. C.; Farkas, O.; Tomasi, J.; Barone, V.; Cossi, M.; Cammi, R.; Mennucci, B.; Pomelli, C.; Adamo, C.; Clifford, S.; Ochterski, J.; Petersson, G. A.; Ayala, P. Y.; Cui, Q.; Morokuma, K.; Malick, D. K.; Rabuck, A. D.; Raghavachari, K.; Foresman, J. B.; Cioslowski, J.; Ortiz, J. V.; Baboul, A. G.; Stefanov, B. B.; Liu, G.; Liashenko, A.; Piskorz, P.; Komaromi, I.; Gomperts, R.; Martin, R. L.; Fox, D. J.; Keith, T.; Al-Laham, M. A.; Peng, C. Y.; Nanayakkara, A.; Gonzalez, C.; Challacombe, M.; Gill, P. M. W.; Johnson, B.; Chen, W.; Wong, M. W.; Andres, J. L.; Gonzalez, C.; Head-Gordon, M.; Replogle, E. S.; Pople, J. A. *Gaussian 98*, revision A.7; Gaussian, Inc.: Pittsburgh, PA, 1998.
(17) Reaction conditions: 15 mL of solvent, $[\mathbf{B}^W] = 1.5$ mmol/L, 1 equiv of acid, room temperature, oxygen- and moisture-free conditions.

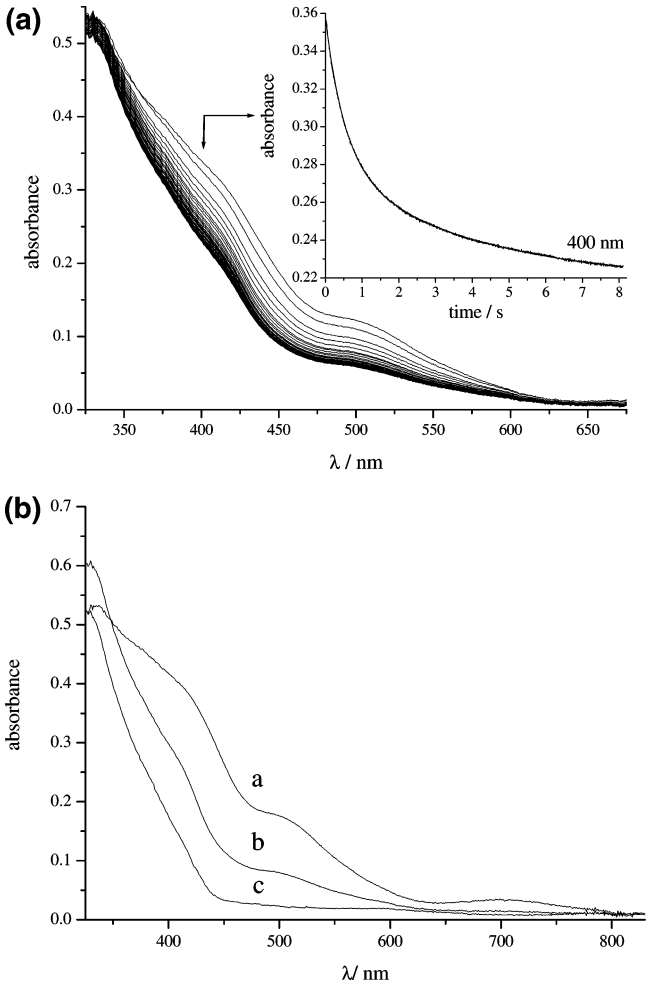

Figure 2. (a) Time evolution of the UV/vis spectra recorded at time intervals of 0.22 s. Experimental conditions: [$\mathbf{B}^{W}$] = 0.053 mM, [$HNEt_3BPh_4$] = 0.32 mM in propionitrile at −70 °C. Inset: Absorbance/time plot showing the evolution of absorbance at 400 nm. (b) Spectra of (a) starting, (b) intermediate, and (c) product species calculated from the rapid-scan measurements in Figure 2a.

(Figure 1), indicating that protonation of $\mathbf{B}^{W}$ in propionitrile also leads to the nitrido complex and piperidine.

Time-dependent spectra of the protonation of $\mathbf{B}^{W}$ (0.053 mM) with $HNEt_3BPh_4$ (0.32 mM) at −70 °C in propionitrile are shown in Figure 2a. The decay of the absorbance at 400 nm exhibits a biphasic character for which $k_{obs(1)} = 1.5 \pm 0.4\ s^{-1}$ and $k_{obs(2)} = 0.35 \pm 0.08\ s^{-1}$. It should be noted, however, that the first spectrum recorded immediately after mixing (see Figure 2b, spectrum a) in comparison to the spectrum of $\mathbf{B}^{W}$ (0.053 mM) and $HNEt_3BPh_4$ (0.32 mM) before mixing (cf. Figure S1, solid line) exhibits about 50% lower absorbance in the spectral range of 350−650 nm. This clearly shows that a fast reaction, which is ascribed to the rapid protonation of $\mathbf{B}^{W}$, has already occurred within the dead time of the stopped-flow instrument. In agreement with Scheme 1, the faster process ($k_{obs(1)}$) is attributed to solvent attack on the protonated intermediate $\mathbf{B}^{W}H^{+}$ and the slower process ($k_{obs(2)}$) to the N−N cleavage reaction of the corresponding solvent-coordinated intermediate EtCN−$\mathbf{B}^{W}H^{+}$. For a 10-fold higher acid concentration, the corresponding values of $k_{obs(1)}$ and $k_{obs(2)}$ are almost identical, i.e., 1.6 ± 0.4 and $0.36 \pm 0.09\ s^{-1}$, respectively. The option of

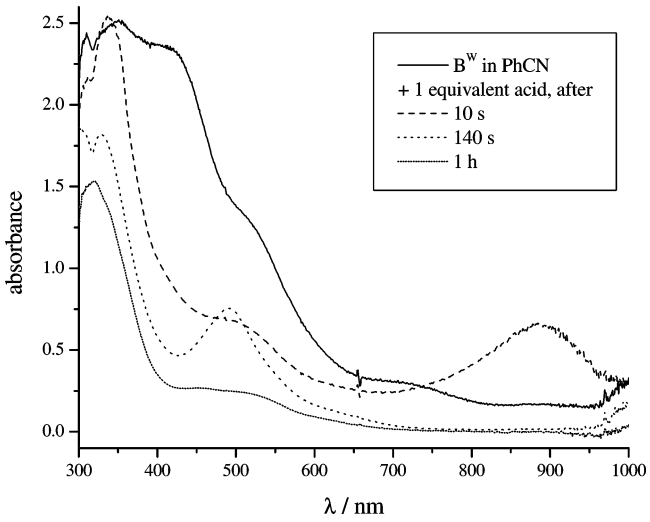

Figure 3. UV− vis spectrum of $\mathbf{B}^{W}$ and of time-dependent protonation products in benzonitrile.

a variable mixing volume ratio was applied for concentrations of $HNEt_3BPh_4$ up to 6 mM, and no changes in the $k_{obs(1)}$ and $k_{obs(2)}$ values could be observed. The independence of $k_{obs(1)}$ from the H^{+} concentration reflects the fact that protonation of $\mathbf{B}^{W}$ to the primary intermediate $\mathbf{B}^{W}H^{+}$ is much faster than solvent attack and already complete upon addition of 6 equiv of acid during the mixing time. A propionitrile solution of $\mathbf{B}^{W}$ was titrated with $HNEt_3BPh_4$, and it was observed that just a small excess of acid is required for complete protonation. The saturation of the initial protonation equilibrium at acid concentrations slightly in excess of the complex concentration has also been established for $\mathbf{B}^{Mo}$.[8] The fact that $k_{obs(2)}$ is also independent of the H^{+} concentration differs from the protonation of $\mathbf{B}^{Mo}$ for which the overall rate constant for N−N cleavage (k_{obs}) was found to depend on the acid concentration.[8]

Calculated spectra for the decay process of compound $\mathbf{B}^{W}$ are given in Figure 2b. It is clearly seen that the spectrum of the solvent-coordinated, protonated intermediate (**b**) observed after the first phase of the decay ($k_{obs(1)}$) has a higher absorbance in the UV region than both the nonsolvated, protonated species observed at "$t = 0$" (i.e., after the dead time of the apparatus) and the final product (**c**). The intermediate in spectrum b is a W(II) complex that is bent at N_α. Its electronic structure (orbital occupancy) is different from that of compound **B** (see below); in particular, the HOMO has changed from a metal-type dσ orbital to a metal-type dπ orbital. Hence, its absorption spectrum is different from that of compound **B** and its protonated derivative. The final product (**c**) (see Figure 2b and spectrum f in Figure 1) is a W(IV) nitrido or imido complex, with a low absorption at 400 nm.

3. Protonation of $\mathbf{B}^{W}$ with $HNEt_3BPh_4$ in Benzonitrile. In benzonitrile, the protolytic N−N cleavage of $\mathbf{B}^{W}$ with $HNEt_3BPh_4$ is dramatically slowed, rendering it possible to follow this process at room temperature. UV/vis spectroscopic monitoring of the reaction course, however, reveals characteristic differences from the results described above (Figure 3). The spectrum of unprotonated $\mathbf{B}^{W}$ in benzonitrile

Scheme 3. Formation of a Dialkylisodiazene Intermediate

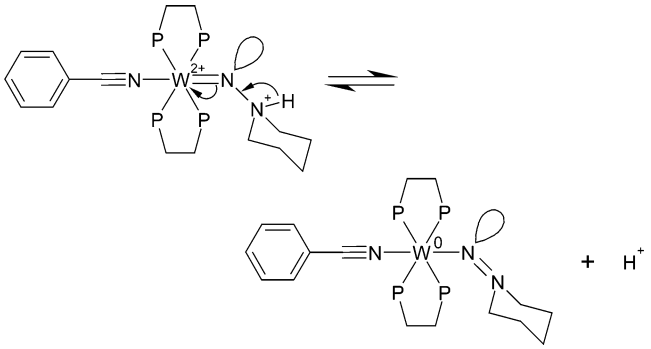

is almost identical to that in propionitrile (Figure S1) or THF (Figure 1). Upon protonation with 1 equiv of acid, an intense band appears at 900 nm that is not observable in propionitrile or in THF. This band subsequently shifts to 500 nm and then, in a much slower process, disappears upon conversion to the final spectrum. These observations obviously reflect changes in the electronic structure of the solvent-coordinated intermediate(s) that are caused by the replacement of propionitrile by benzonitrile. Because benzonitrile is more π-accepting than acetonitrile and propionitrile, we attribute the intermediate with the unusual 900-nm band to a benzonitrile-coordinated, bent W(0) dialkylisodiazene complex (Scheme 3). In this intermediate, which is stabilized by two π-back-bonding interactions to the benzonitrile ligand, the protonated hydrazidium ligand has transferred two electrons to the metal center, possibly under loss of its proton; at the same time, the N−N interaction is enhanced to a double bond. This explains why N−N cleavage is dramatically slowed. A charge-transfer (CT) transition could occur in this intermediate from the metal center to the π^* orbital of the bent isodiazene ligand, in analogy to the low-energy CT band observed in Fe-diazene complexes.[18]

The spectrum of the second intermediate already is very similar to that of the final product, except for the more pronounced absorption band around 500 nm. The intensity of this band has decreased in the spectrum of the final product (after 1 h). Interestingly, this band is not present in the spectrum of the benzonitrile nitrido complex $[W(N)(PhCN)(dppe)_2]^+$ prepared independently (cf. Figure S2). Only after several hours does this band disappear and the spectrum of the reaction mixture approach that of $[W(N)(PhCN)(dppe)_2]^+$. We therefore attribute the 500-nm band to a benzonitrile-coordinated, bent dialkylhydazidium intermediate with a very long N−N bond where complete N−N cleavage appears to be hindered by the electron-withdrawing effect of the coordinated benzonitrile ligand.

To confirm that N−N splitting of $\mathbf{B}^{W}$ takes place in benzonitrile, ^{15}N NMR spectroscopy was employed. The spectrum of $\mathbf{B}^{W}$ in benzonitrile exhibits a doublet at −18 ppm that is assigned to N_β, split by coupling with N_α (Figure S3). The signal of N_α is not observed, presumably because of broadening effects. Upon addition of $HLutBPh_4$, the signal at −18 ppm disappears, and two signals at −341.17 and −352.8 ppm are detected. These are assigned to piperidine and piperidinium, respectively (Figure S4).[19] It thus can be concluded that N−N splitting takes place in benzonitrile as well, but at a strongly decreased rate as compared to acetonitrile and propionitrile.

4. Theoretical Treatment. To obtain further insight into the mechanism of the protolytic N−N bond cleavage of compound $\mathbf{B}^{W}$, DFT was employed. As described in the accompanying article,[9] geometry optimization of a slightly simplified model $\tilde{\mathbf{B}}$ was found to closely match the experimentally observed geometry of $\mathbf{B}^{W}$. The HOMO of $\tilde{\mathbf{B}}$ containing two additional electrons compared to its precursor $\tilde{\mathbf{A}}$ corresponds to a linear combination of the metal d_σ orbital with a ligand orbital having N−N σ^* character, inducing a weakening of the N−N bond. Protonation of $\mathbf{B}^{W}$ was then simulated by attaching a proton to the N_β atom of the dialkylhydrazido(2−) ligand of $\tilde{\mathbf{B}}$ in a geometry derived from that of piperidine (HNC_5H_{10}). This generates structure $\tilde{\mathbf{B}}H^+$, which is a model for the alkylhydrazidium species $\mathbf{B}^{W}H^+$ (cf. Scheme 1). Importantly, global geometry optimization of this structure leads to separation into piperidine and the nitrido complex, corresponding to an exothermic (−41 kcal/mol) and spontaneous N−N cleavage process of $\mathbf{B}^{W}$ after protonation at N_β (Scheme 4). Figure 4a displays a relaxed potential energy surface (rPES) for the N−N splitting process of $\tilde{\mathbf{B}}H^+$, demonstrating that this reaction occurs without a barrier. The HOMO of $\tilde{\mathbf{B}}H^+$ containing a N−N antibonding interaction (cf. the accompanying article[9]) thereby evolves to the lone pair of piperidine. The five-coordinate nitrido complex will coordinate a solvent molecule after completion of the N−N cleavage process. The N−N bond-splitting reaction of $\tilde{\mathbf{B}}H^+$ thus can be considered as an orbital- and symmetry-allowed, heterolytic cleavage process that is associated with an oxidation of the metal center from +II to +IV. Note that this process occurs without significant bending of $\tilde{\mathbf{B}}H^+$ at N_α.

So far, the solvent has not been included in the calculation. However, as shown experimentally, solvent attack on the protonated derivatives of the bialkylated complexes $\mathbf{B}^{Mo}$ and $\mathbf{B}^{W}$ plays an important role in the N−N splitting reaction, at least in nitrile solvents. To obtain further information on this reaction mode, bonding of acetonitrile (R = Me) to the protonated intermediate $\mathbf{B}^{W}H^+$ was simulated by DFT, leading to the model MeCN−$\tilde{\mathbf{B}}H^+$. Attachment of the MeCN ligand to the linear molecule $\tilde{\mathbf{B}}H^+$ initially leads to an increase of energy (+16 kcal/mol; Scheme 4). Then, this structure bends at N_α, causing a change of one of the in-plane p-donor orbitals of the NNR_2 group (π_h^*) to a lone pair at N_α and a conversion of the HOMO of $\tilde{\mathbf{B}}H^+$ from a d_σ- to a d_π-type metal orbital. Importantly, this HOMO contains an antibonding contribution of the lone pair at N_α and a p orbital at N_β that is directed along the N−N axis and is antibonding with respect to the lone pair at N_α (Chart 2). Further geometry optimization of structure MeCN−$\tilde{\mathbf{B}}H^+$ leads to separation into the nitrido complex and piperidine,

(18) Lehnert, N.; Wiesler, B.; Tuczek, F.; Hennige, A.; Sellmann, D. *J. Am. Chem. Soc.* **1997**, *119*, 8869−8878.

(19) Duthaler, R. O.; Roberts, J. D. *J. Am. Chem. Soc.* **1978**, *100* (12), 3882.

Scheme 4. Protonation Pathways and Product Energies in Relation to $\tilde{\mathbf{B}}H^+$ (kcal/mol; *partial optimization; N−N distance fixed at 1.5 Å)

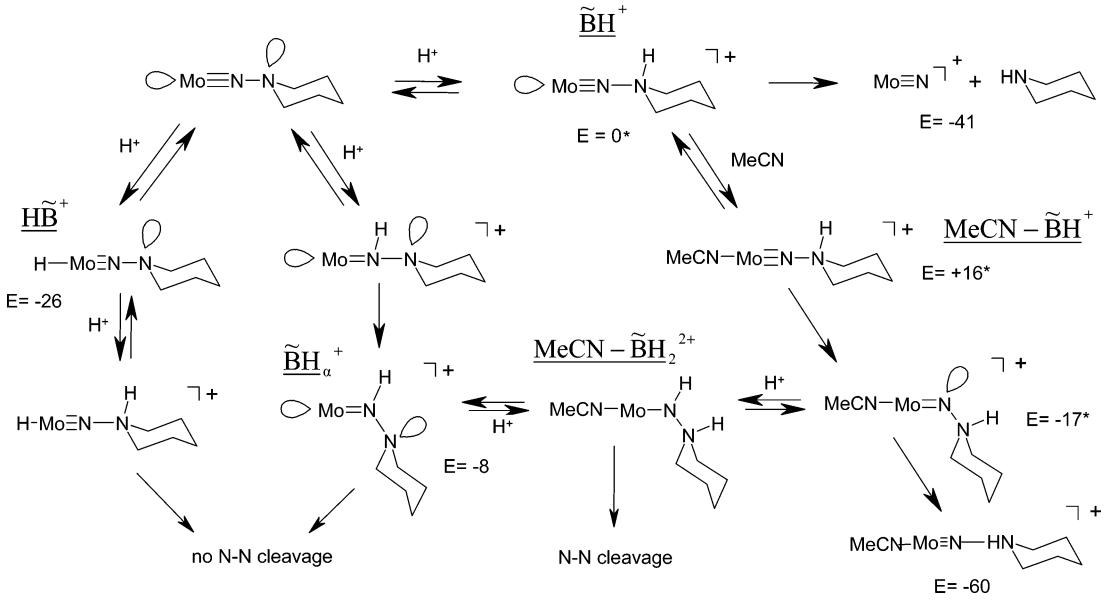

indicating that the nitrile-coordinated intermediates RCN−$\mathbf{B}^{W}H^+$ spontaneously cleave the N−N bond just as their nonsolvated counterpart does (Scheme 4). In analogy to the N−N cleavage process of this intermediate, the HOMO of structure MeCN−$\tilde{\mathbf{B}}H^+$ is thereby converted to the N lone pair of piperidine. Again, the N−N antibonding interaction in the HOMO of the doubly reduced, protonated intermediate is essential for this spontaneous, heterolytic N−N cleavage process.

With respect to the retardation of the N−N splitting reaction of $\mathbf{B}^{W}$ in benzonitrile (cf. section III.A.3), it also appeared of interest to treat the benzonitrile-coordinated, N_β-protonated intermediate PhCN−$\mathbf{B}^{W}H^+$ by DFT. Geometry optimization of the corresponding model MeCN−$\tilde{\mathbf{B}}H^+$ initially leads to bending at *both* N_α of the NNR_2 group *and* the nitrogen atom of the nitrile ligand, indicating some charge transfer to the benzonitrile ligand. Further DFT geometry optimization leads to N−N cleavage, suggesting that spontanous N−N splitting occurs in benzonitrile as well. This is in agreement with the ^{15}N NMR spectroscopic evidence for N−N cleavage of $\mathbf{B}^{W}$ in this solvent (vide supra) and the similar findings of Henderson et al. for $\mathbf{B}^{Mo}$.[8] The observed decrease of the N−N splitting rate of $\mathbf{B}^{W}$ in benzonitrile as compared to the rates in acetonitrile and propionitrile must be a consequence of the delocalization of electron density into the π^* orbitals of the benzonitrile ligand, which is also evident from the unusual features detected by UV/vis spectroscopic monitoring of the protonation reaction (Figure 3). Back-bonding into the benzonitrile ligand acts to decrease the basicity on N_β, possibly causing a partial deprotonation of PhCN−$\tilde{\mathbf{B}}H^+$ (cf. Scheme 3), and introduces a barrier for N−N cleavage (which is not evident in the calculation based on the simplified model); both factors effectively slow the N−N cleavage process.

Reduced basicity of the benzonitrile-coordinated species PhCN−$\mathbf{B}^{Mo}H^+$ (however, at N_α) has also been invoked by Henderson et al.[8] to explain that, for this solvent, no acid-assisted N−N cleavage of $\mathbf{B}^{Mo}H^+$ could be detected. This pathway was hypothesized to involve a second protonation at N_α, leading to the doubly protonated species RCN−$\mathbf{B}^{Mo}H_2^{2+}$ (R = Me, Et), which undergo N−N splitting with a rate constant k_5 (Scheme 1). Geometry optimization of the corresponding doubly protonated, acetonitrile-coordinated structure MeCN−$\tilde{\mathbf{B}}H_2^{2+}$, however, was found to leave the N−N bond intact. To obtain more information on the energetics of N−N cleavage, a relaxed potential energy scan (rPES) along the N−N coordinate was performed (Figure 4b). Interestingly, the rPES shows an exothermic splitting process of the N−N bond (approximately −45 kcal/mol) with a very small activation barrier (∼1 kcal/mol). Upon elongation of the N−N bond, the N_α proton first flips into a position between N_α and N_β. Then proton transfer from N_α to N_β occurs.[20] This theoretical result supports the presence of an alternative, acid-assisted N−N cleavage pathway for the intermediates RCN−$B^{M}H^+$ (M = Mo, W), associated with the rate constant k_5 in Scheme 1. Experimentally, the second protonation (at N_α) is characterized by an equilibrium constant K_3, making the overall rate of this decay path effectively dependent on the product k_5K_3. The fact that no dependence of the N−N cleavage rate on the acid concentration is observed for the protolytic N−N cleavage of $\mathbf{B}^{W}$ in propionitrile can then be explained in two ways: (i) K_3 is already saturated by a small excess of acid (exactly as for the protonation equilibrium at N_β), and the observed N−N cleavage process is dominated by the k_5 pathway; (ii) K_3 is so small that the k_5 route is unimportant in comparison to the k_4 pathway. On the basis of the observation that the N−N cleavage reaction of $\mathbf{B}^{W}$ is much faster than of that $\mathbf{B}^{Mo}$, we assume that alternative i is correct. This would be in agreement with the general rule that tungsten complexes are easier to protonate than their molybdenum counterparts.[21]

(20) Of course, the resulting nitrido complex will be protonated in the presence of an excess of acid.
(21) Henderson, R. A.; Leigh, G. J.; Pickett, C. *Adv. Inorg. Chem. Radiochem.* **1983**, *27*, 197−292.

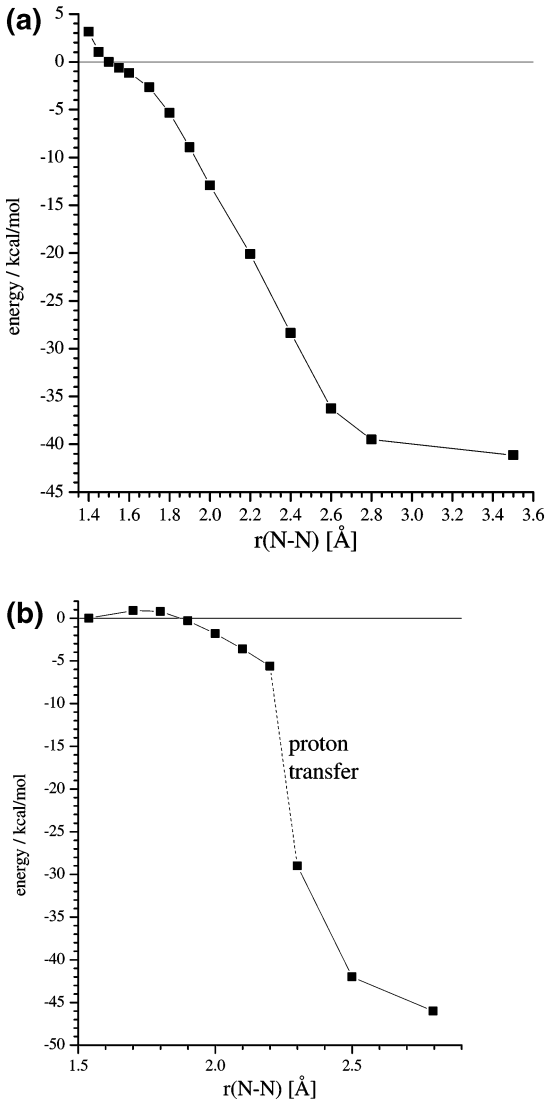

Figure 4. rPES for N−N splitting reactions of (a) $\tilde{\mathbf{B}}H^+$ and (b) MeCN−$\tilde{\mathbf{B}}H_2^{2+}$.

Chart 2. Contour Plot of HOMO from MeCN−BH^+

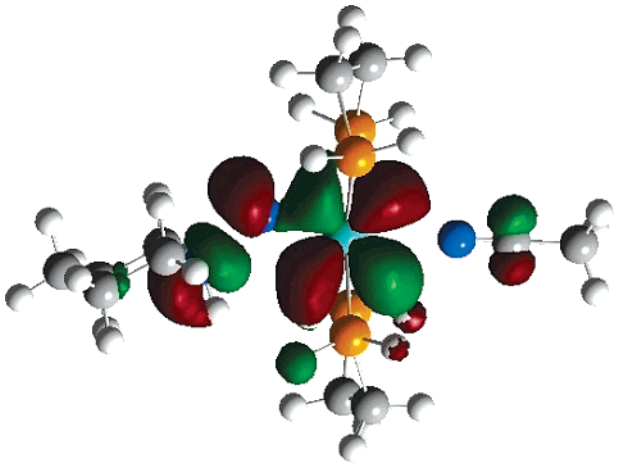

With respect to further mechanistic scenarios for the N−N splitting of $\mathbf{B}^W$, initial protonation at the metal has to be considered. As shown in the accompanying article,[9] the HOMO of this molecule exhibits a large lobe toward the open side of the complex, making this a potential site for attack by H^+ as well. For this reason, bonding of a proton to $\tilde{\mathbf{B}}$ was simulated by DFT, leading to the *metal*-protonated species $H\tilde{\mathbf{B}}^+$. After geometry optimization, the energy of this structure was found to be 26 kcal/mol lower than that of the N_β-protonated species $\tilde{\mathbf{B}}H^+$ (Table 1), and the N−N bond was left intact. In this case, however, N−N cleavage (even after further protonation at N_β) is prevented by formation of a hydrido group trans to the NNR_2 ligand that consumes the electrons in the HOMO of $\mathbf{B}^W$ necessary for N−N cleavage. Metal protonation thus would correspond to a thermodynamically favorable, but nonproductive step in the overall reaction scheme, lowering the observed N−N splitting rate. It must be taken into account, on the other hand, that protonation of $\mathbf{B}^W$ proceeds by proton transfer from undissociated acid or protonated solvent,[8] imposing some steric requirements on this process. A space-filling representation of the structure of $\mathbf{B}^W$ shows that the metal is highly shielded by the phenyl groups of the dppe ligands (Figure 5). Moreover, upon protonation at N_β, solvent attack on $\mathbf{B}^W$ is rapid in coordinating solvents (vide supra). Both effects would act to kinetically disfavor protonation at the metal center.

Table 1. Energies of Protonated Intermediates

intermediate	energy (a.u.)	relative energy (kcal/mol)
$\tilde{\mathbf{B}}H^{+\,a}$	−561.878083	0
$H\tilde{\mathbf{B}}^{+\,b}$	−561.920119	−26
$\tilde{\mathbf{B}}H_\alpha{}^{+\,b}$	−561.890336	−8
MeCN−Mo≡N^+ + $C_5H_{11}N^b$	−561.9743466	−60
Mo≡N^+ + $C_5H_{11}N^b$	−561.943661	−41

[a] N−N distance fixed at 1.50 Å, partially optimized. [b] Fully optimized.

Judging from the finding that N_α is more negative than N_β in $\mathbf{B}^W$,[22] initial protonation of $\mathbf{B}^W$ should be possible at N_α as well. DFT geometry optimization of the corresponding intermediate $\tilde{\mathbf{B}}H_\alpha{}^+$ leads to bending of the NNR_2 group at N_α, leaving the N−N bond intact (relative energy = −8 kcal/mol). As evidenced by a DFT PES, elongation of the N−N bond by 3 Å from the optimized value is endothermic by 70 kcal/mol (Figure S5); protonation at N_α therefore does not lead to N−N splitting under ambient conditions. This corresponds to the fact that heterolytic cleavage after protonation at N_α would lead to a negatively charged (piperidide) fragment and the imido complex, which energetically is highly unfavorable. To mediate N−N cleavage, the proton therefore has to shift from N_α to N_β, which can be effected by a combination of deprotonation/reprotonation steps (Scheme 4).

To conclude, protonation at N_β is found by DFT to induce an exothermic and activationless N−N cleavage process, in both the unsolvated and the solvent-coordinated primary intermediate $\mathbf{B}^WH^+$ and RCN−$\mathbf{B}^WH^+$. From the literature data and our own experimental results, solvent attack on the primary intermediate $\mathbf{B}^WH^+$ is faster than N−N splitting of the solvated intermediate RCN−$\mathbf{B}^WH^+$. The same probably holds for the N−N cleavage process of the unsolvated intermediate $\mathbf{B}^WH^+$; i.e., this direct decay channel also

(22) cf. Table 11 of the accompanying article.[9]

Table 2. Comparison of Calculated Structures **I**−**VI** with Experimental Results

complex[a]		data source[b]	bond lengths (Å) N−N	Mo−N	Mo−N_{AD}[c,d]	MoN_{AM}[e]	angles (deg) MoNN	N_{AM}MoN
$[N_3N]Mo^{III}N_2$ $S = 1/2$	**I**	X-ray	1.06	1.96	1.98	2.19	179.2	179.8
		opt	1.17	1.97	1.99	2.25	178.5	178.5
$[N_3N]Mo^{VI}NNH_2^+$	**II**	opt	1.32	1.78	1.96	2.31	177.0	177.6
$[N_3N]Mo^{V}NNH_2$	**III**	opt	1.35	1.86	1.99	2.34	142.0	176.6
$[N_3N]Mo^{IV}NNH_2^-$ $S = 0$	**IV**	opt	1.42	1.82	2.03	2.49	141.0	159.8
$[N_3N]Mo^{V}NNH_3^+$	**V**	opt	1.57	1.85	1.96	2.35	128.9	179.2
$[N_3N]Mo^{IV}N$	**VI**	X-ray	−	1.65	2.00	2.40	−	179.1
		opt	−	1.70	1.98	2.56	−	175.2

[a] $[N_3N] = (HNCH_2CH_2)_3N^{3-}$. [b] opt = optimized structure, X-ray data taken from ref 11c. [c] Data are averaged for simplification. [d] N_{AD} is the nitrogen atom of the Amides. [e] N_{AM} is the nitrogen atom of the amine.

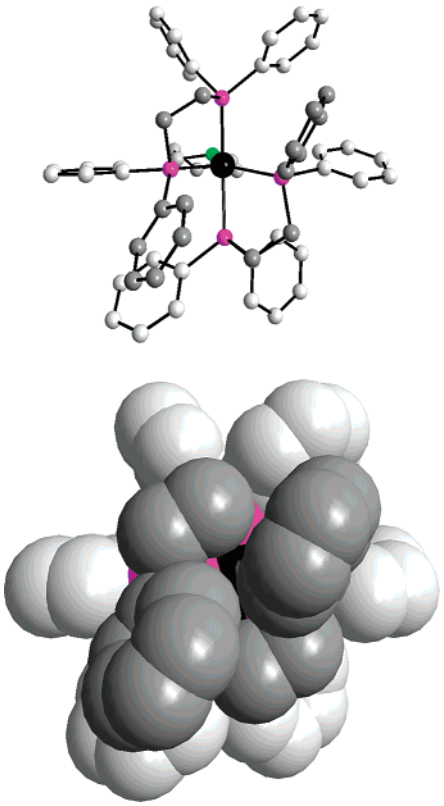

Figure 5. Structure of $\mathbf{B}^{W}$: view of the shielded metal side.

appears to be slower than solvent attack on the protonated intermediate $\mathbf{B}^{W}H^+$. Direct N−N cleavage of $\mathbf{B}^{W}H^+$ thus appears to be intercepted by solvent attack in coordinating solvents. N−N cleavage of the doubly protonated intermediate (at N_α *and* N_β), finally, is theoretically predicted to occur in an almost activationless fashion as well. In contrast to $\mathbf{B}^{Mo}$, the protonation preequilibrium of this decay channel appears to be saturated for $\mathbf{B}^{W}$ in the presence of an excess of acid. Under such conditions, the observed N−N cleavage process of $\mathbf{B}^{W}$ is therefore dominated by the decay of the doubly protonated intermediate.

B. Protonation, Reduction, and N−N Cleavage of Dinitrogen in [$Mo^{III}(N_2)$(triamidoamine)]. 1. Introductory Remarks. DFT calculations and geometry optimizations have been performed for the complexes $[N_3N]Mo^{III}(N_2)$ (**I**) and $[N_3N]Mo^{VI}(NNH_2)^+$ (**II**), which are models for the respective N_2 and NNH_2 intermediates of the [$HIPTN_3N$]-Mo fragment (Chart 1). Moreover, DFT calculations have been performed on the hypothetical intermediates $[N_3N]$-$Mo^{V}(NNH_2)$ (**III**), $[N_3N]Mo^{IV}(NNH_2)^-$ (**IV**), and $[N_3N]$-$Mo^{V}(NNH_3)^+$ (V) ([N_3N] = triamidoamine; the terphenyl substitutents of $HIPTN_3N$ have been replaced by hydrogen atoms in these calculations). A comparison between calculated bond distances/angles and experimentally determined structural data is given in Table 2. Calculated frequencies are compared with available spectroscopic data in Table 3. NPA charges for the calculated structures are given in Table 4; energies and decompositions for important orbitals of **I**, **III**, and **V** are collected in Tables 5−7.

Table 3. Comparison of Calculated and Observed Frequencies of Complexes **1**, **2**, and **6** with Models **I**, **II**, **V**, and **VI**

complex		mode	experimental[a,b] ^{14}N	experimental[a,b] ^{15}N	B3LYP[a] ^{14}N	B3LYP[a] ^{15}N
$[N_3N]Mo^{III}N_2$ $S = 1/2$	**I**	ν(N−N)	1990	1924	1911	1844
$[N_3N]Mo^{VI}NNH_2^+$	**II**	$\nu(N-H)_{as}$	3379	3370	3691	3679
		$\nu(N-H)_{s}$	3274	3270	3542	3538
		ν(N−N)	−	−	1487	1443
$[N_3N]Mo^{V}NNH_3^+$	**V**	ν(N−N)	−	−	467	455
		ν(Mo−N)	−	−	712	700
$[N_3N]Mo^{IV}N$	**VI**	ν(Mo−N)	1013	986	1090	1059

[a] In cm^{-1}. [b] Data taken from ref 11c.

Table 4. NPA Charges of Model Complexes **I**−**VI**

complex[a]		atom Mo	Nα	Nβ	H[b]	N_{AD}[b,c]	N_{AM}[d]
$[N_3N]Mo^{III}N_2$ $S = 1/2$	**I**	1.10	−0.18	−0.05	−	−0.90	−0.56
$[N_3N]Mo^{VI}NNH_2^+$	**II**	1.26	−0.17	−0.57	0.43	−0.82	−0.58
$[N_3N]Mo^{V}NNH_2$	**III**	1.19	−0.37	−0.65	0.38	−0.91	−0.58
$[N_3N]Mo^{IV}NNH_2^-$ $S = 0$	**IV**	0.87	−0.49	−0.71	0.33	−0.94	−0.57
$[N_3N]Mo^{V}NNH_3^+$	**V**	1.31	−0.49	−0.67	0.45	−0.86	−0.58
$[N_3N]Mo^{IV}N$	**VI**	1.23	−0.42	−	−	−0.89	−0.60

[a] $[N_3N] = (HNCH_2CH_2)_3N^{3-}$. [b] Charge for each H atom. [c] N_{AD} is the nitrogen atom of the amides. [d] N_{AM} is the nitrogen atom of the amine.

2. N_2 Complex (I). As a starting point for the investigation of the N−N cleavage process in the Mo triamidoamine system, the electronic structure of the dinitrogen complex $[N_3N]Mo^{III}(N_2)$ (**I**) is determined. A DFT study on **I** has been presented before.[23] The d-orbital energy level scheme of **I** is typical for a trigonal-bipyramidal complex (Figure 6 and Table 5). The $d_{x^2-y^2}$ and d_{xy} orbitals are shifted to high energy by strong σ- and π-antibonding interactions of the amide p-donor orbitals within the trigonal plane. At lower energy are found the degenerate d_{xz} and d_{yz} orbitals, which are

(23) Cui, Q.; Musaev, D. G.; Svensson, M.; Sieber, S.; Morokuma, K. *J. Am. Chem. Soc.* **1995**, *117*, 12366.

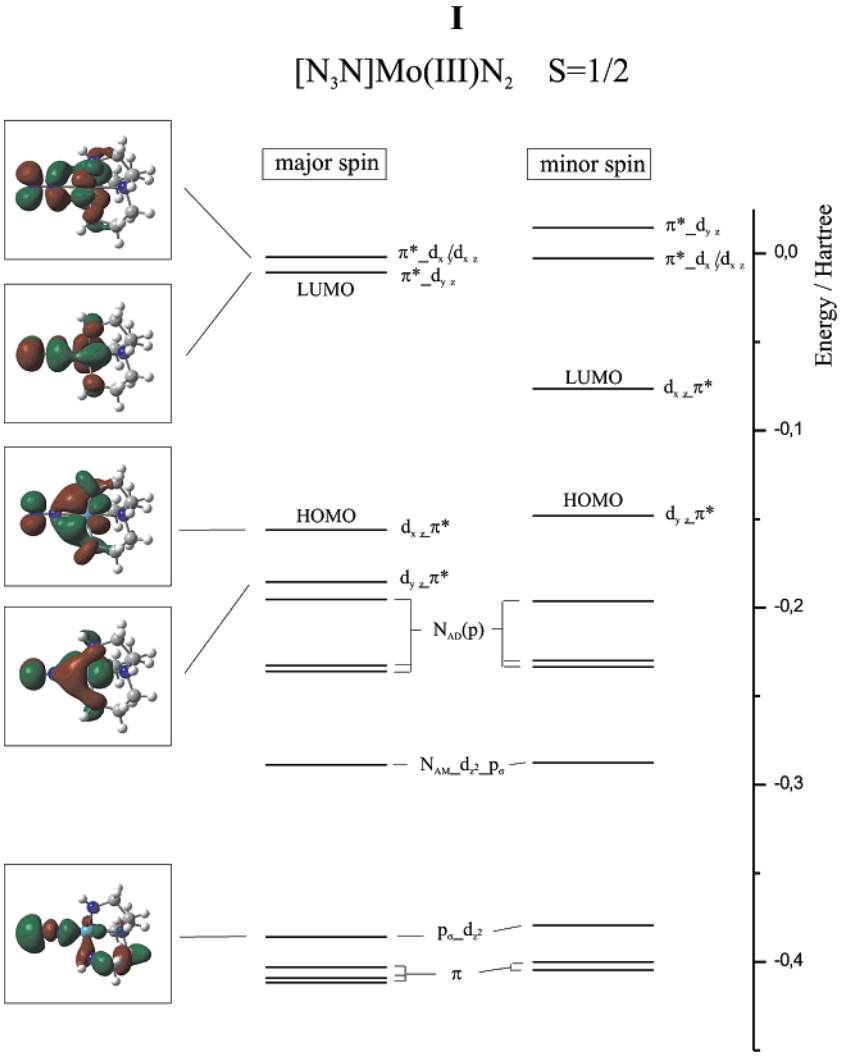

Figure 6. MO diagram and contour plots of important molecular orbitals of **I**.

Table 5. Charge Contribution of Model Complex **I**

orbital	label	energy (hartree)	α spin charge decomposition				
			Nα	Nβ	Mo	N_{AD}	N_{AM}
π^*–d_{xy}/d_{xz}	56	−0.00191	19	19	29	12	1
π^*–d_{z^2}/d_{yz}	55	−0.01069	27	26	21	8	1
d_{xz}–π^*	54	−0.15617	2	19	61	9	0
d_{yz}–π^*	53	−0.18548	1	15	65	10	0
N_{AD}	52	−0.19524	0	0	2	78	1
N_{AD}	51	−0.23272	0	0	22	56	1
N_{AD}	50	−0.23589	0	0	17	62	0
N_{AM}–p_σ–d_{z^2}	49	−0.28873	4	2	7	2	55
p_σ–d_{z^2}	40	−0.38605	19	53	6	6	1
π	39	−0.40297	50	34	3	1	0
π	38	−0.40916	15	15	2	21	7
π	37	−0.41176	33	26	3	10	3

nonbonding with respect to the amide orbitals but back-bonding with respect to the dinitrogen orbitals. Population of these orbitals with the three electrons of Mo(III) gives rise to a ^{2}E ground state. NBO charge analysis indicates a charge of −0.18 at N_α and −0.05 at N_β, comparable to those of Mo/W dinitrogen complexes with diphosphine coligands.[24] At 1.17 Å, the calculated N−N bond length is larger than experimentally determined (1.06 Å), indicating that the activation of this ligand predicted by the calculation is too large. Correspondingly, the N−N stretching frequency is calculated at 1911 cm^{-1}, lower than experimentally observed (1990 cm^{-1}).

3. Mo(VI) NNH_2 Complex (II). Bonding of two protons to the dinitrogen complex **I** along with one-electron reduction gives the NNH_2 complex $[N_3N]Mo(NNH_2)^+$ (**II**). The HOMO of this species is a nonbonding linear combination of amide lone pairs (Figure S6). As described earlier, the planar NNH_2 ligand has an in-plane π_h^* orbital that mostly corresponds to a p-donor orbital at N_α, whereas the out-of plane orbital π_v^* has N−N π^* character.[24] Below the HOMO are the bonding combinations of Mo d_{yz} and d_{xz}/d_{xy} with the NNH_2 π_v^* and π_h^* orbitals, respectively, which are primarily of *ligand* character (Table S1); LUMO and LUMO + 1 are formed by the corresponding metal−ligand anti-bonding combinations. The electrons associated with metal−ligand π-bonding can therefore be assigned to the ligand, corresponding to a Mo(VI)/hydrazido(2−) formulation. However, NBO charge analysis indicates that the total charge on the NNH_2 ligand is slightly positive. This indicates a strong donation of the 2− ligand charge back to the Mo(VI) metal center, effectively leading to a neutral bound isodiazene

(24) Lehnert, N.; Tuczek, F. *Inorg. Chem.* **1999**, *38*, 1671.

III

$[N_3N]Mo(V)NNH_2$

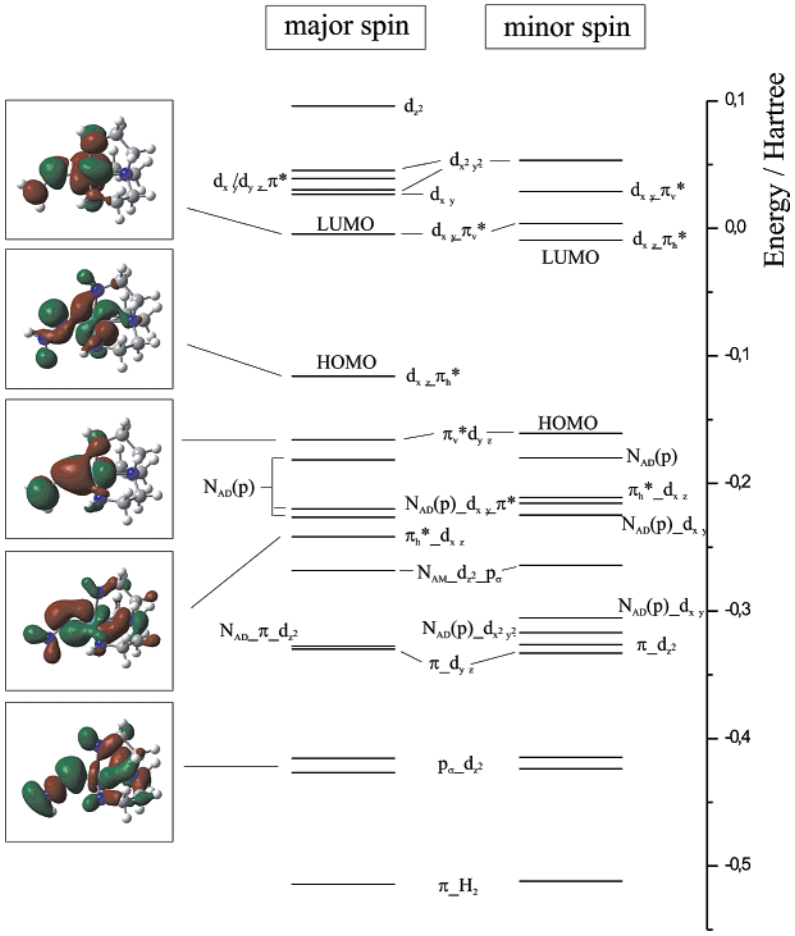

Figure 7. MO diagram and contour plots of important molecular orbitals of **III**.

species. This also agrees with the N−N bond length of 1.32 Å and the N−N stretching frequency of 1487 cm^{-1}, which both are indicative of a N−N double bond.[18,24] Complex **II** therefore corresponds to a Mo(VI) hydrazido(2−) species that is subject to large ligand → metal charge donation because of the highly positive charge on the metal center.

4. Mo(V) NNH_2 Complex (III). Transfer of one electron to **II** gives the putative neutral $S = {}^1/_2$ Mo(V) species $[N_3N]$-$Mo(NNH_2)$ (**III**). DFT geometry optimization of this structure reveals bending of the NNH_2 group at N_α in the NH_2 plane, causing conversion the π_h^* p-donor orbital to a lone pair at N_α (for simplicity, we retain the π_h^* formulation for this orbital). The SOMO of **III** is a metal d_{xz} orbital with an antibonding contribution from the lone pair at N_α (d_{xz}–π_h^*, Figure 7 and Table 6). The corresponding antibonding combination with π_v^*, d_{xy}–π_v^*, is unoccupied. Because of population of the SOMO that is metal−ligand antibonding but N−N nonbonding, the metal−N bond of **III** is elongated by 0.08 Å with respect to that in **II**, whereas the N−N bond length is increased by only 0.03 Å.

5. Mo(IV) NNH_2 Complex (IV) and Its Protolytic N−N Cleavage. Addition of one electron to **III** generates the doubly reduced NNH_2 complex $[N_3N]Mo^{IV}(NNH_2)^-$ (**IV**), which, upon protonation, cleaves the N−N bond. The two electrons of the Mo(IV) configuration give rise to $S = 0$ and $S = 1$ states, the former being found at lower energy

Table 6. Charge Contribution of Model Complex **III**

orbital	label	energy (hartree)	α spin charge decomposition					
			Nα	Nβ	Mo	H	N_{AD}	N_{AM}
d_{z^2}	63	0.09590	9	3	27	3	5	13
$d_{x^2-y^2}$	61	0.04551	4	1	57	1	18	0
d_{xy}/d_{yz}–π^*	60	0.03909	7	3	60	1	12	0
$d_{x^2-y^2}$	59	0.03026	0	0	79	0	6	0
d_{xy}	58	0.02681	0	1	79	0	6	0
d_{xy}–π_v^*	56	−0.00448	19	8	40	0	11	1
d_{xz}–π_h^*	55	−0.11599	18	5	49	5	9	1
π_v^*–d_{yz}	54	−0.16575	13	30	42	0	8	0
N_{AD}(p)	53	−0.18145	0	0	1	0	77	1
N_{AD}(p)	52	−0.21997	4	0	13	1	61	1
N_{AD}(p)	51	−0.22645	4	1	17	1	56	1
π_h^*–d_{xz}	50	−0.24180	34	2	30	7	4	13
N_{AM}–d_{z^2}–p_σ	49	−0.26819	12	1	9	2	2	46
N_{AD}–π–d_{z^2}	46	−0.32755	6	10	12	0	39	3
π–d_{yz}	45	−0.32986	25	43	7	0	11	1
p_σ	37	−0.41564	12	6	4	1	11	14
p_σ–d_{z^2}	36	−0.42684	40	20	13	2	6	5
π−H_2	29	−0.51441	6	65	1	26	0	0

V

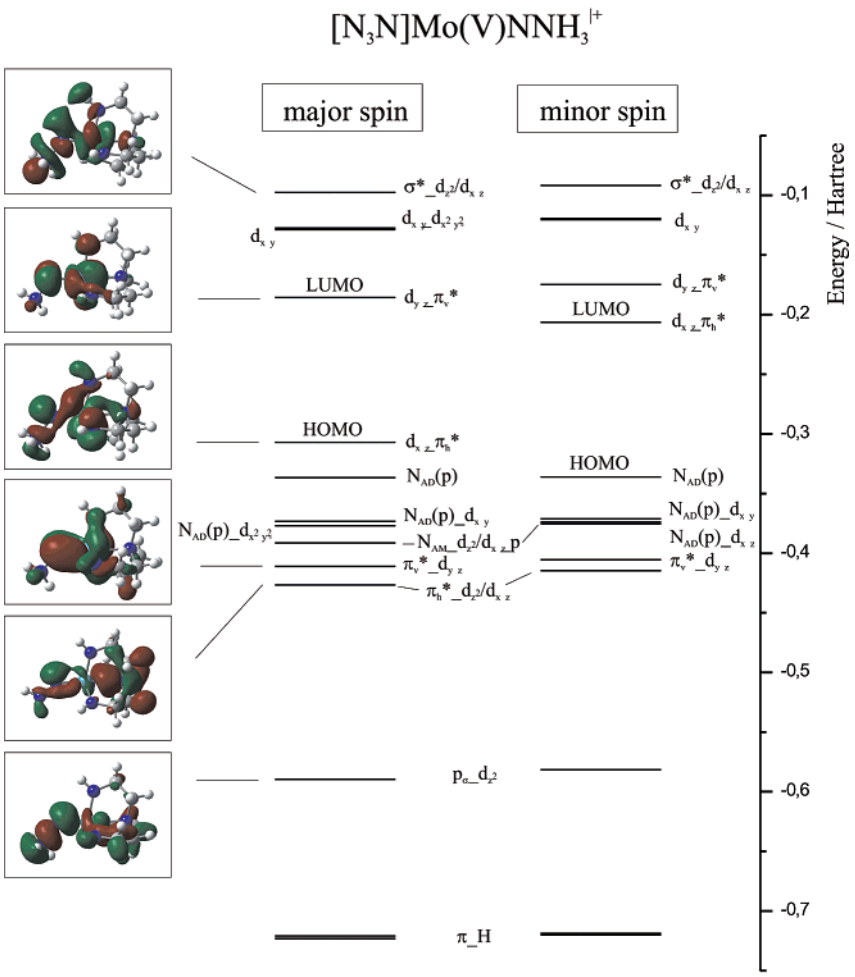

Figure 8. MO diagram and contour plots of important molecular orbitals of **V**.

(9.39 kcal mol^{-1}). Geometry optimization of the $S = 0$ complex leads to a doubly bent NNH_2 ligand (Scheme 2). The HOMO of **IV** is an antibonding combination of a metal d_{xz} orbital with the lone pair at N_α derived from π_h^*. Moreover, this orbital contains a contribution of a N_β p orbital along the N−N bond that is antibonding to the lone pair at N_α (Figure S7). At lower energy is found the bonding combination of the out-of-plane π_v^* with the metal d_{yz} orbital, which is of primarily ligand character (Table S2). This bonding description would correspond to a Mo(IV) hydrazido(2−) formulation for **IV**. This is supported by a N−N bond length of 1.42 Å, indicative of N−N single bond character. NBO charge analysis gives a negative charge of −0.6 for the NNH_2 group, corresponding to back-donation of −1.4 charge units from this ligand to the Mo(IV) metal center.

If a proton is added to model **IV** at N_β, spontaneous N−N cleavage takes place upon geometry optimization and the separate components ammonia and nitrido complex are obtained. Judging from the above bonding description, this corresponds to a heterolytic N−N cleavage process proceeding by two-electron transfer from the HOMO of the protonated derivative of **IV** to the lone pair of NH_3, which is preformed in the HOMO of **IV**. The triplet state of **IV** has not been included in this treatment because it is higher in energy than the singlet state (vide supra) and requires an intersystem crossing along the N−N cleavage path to give the diamagnetic products.

6. Mo(V) NNH_3 Complex (V) and Its Reductive N−N Cleavage. As an alternative to the protolytic N−N cleavage process described above, one proton can be added to **III**, leading to the NNH_3 complex $[N_3N]Mo^V(NNH_3)^+$ (**V**; Scheme 2). Exactly as for **III**, structure **V** has a NNH_3 ligand bent at N_α. The single d electron is contained in the SOMO ⟨55⟩ of **V**, which, as in the case of **III**, is an antibonding combination of a metal orbital with the lone pair at N_α derived from π_h^* (Figure 8, Table 7). Importantly, this orbital also contains a p orbital at N_β directed along the N−N bond, effectively leading to a N−N antibonding interaction with the lone pair at N_α. This is relevant to the N−N splitting process considered below. The other p-donor orbital at N_α of the NNH_3 group that is derived from the out-of-plane orbital π_v^* is involved in a π-bonding fashion with d_{yz} in MO ⟨50⟩.

As indicated by the calculated bond distances, both the N−N and the metal−N bonds are greatly elongated in this

Table 7. Charge Contribution of Model Complex **V**

orbital	label	energy (hartree)	α spin charge decomposition					
			Nα	Nβ	Mo	H	N_{AD}	N_{AM}
$\sigma^*-d_{z^2}/d_{xz}$	60	−0.09762	33	17	32	3	5	3
$d_{xy}/d_{x^2-y^2}$	59	−0.12755	5	14	47	9	17	0
d_{xy}	58	−0.12888	3	2	46	2	30	0
$d_{yz}/d_{xy}-\pi_v^*$	56	−0.18574	19	1	52	3	13	0
$d_{xz}-\pi_h^*$	55	−0.30706	18	14	43	1	12	4
$N_{AD}(p)$	54	−0.33664	3	1	4	1	75	1
$N_{AD}(p)-d_{xy}$	53	−0.37326	18	0	12	1	51	2
$N_{AD}(p)d_{x^2-y^2}$	52	−0.37691	8	0	13	1	51	6
$N_{AM}-d_{xz}$	51	−0.39143	14	2	24	1	7	33
$\pi_v^*-d_{yz}$	50	−0.41104	38	1	35	2	11	0
$\pi_h^*-d_{z^2}/d_{xz}$	49	−0.42665	37	2	20	2	4	16
$p_\sigma-d_{z^2}$	36	−0.58954	32	32	12	1	7	0
$\pi-H_2$	29	−0.72094	1	74	0	24	0	0
$\pi-H_3$	28	−0.72307	2	73	0	24	0	0

intermediate (1.85 and 1.57 Å, respectively), corresponding to population of the metal−N and N−N antibonding SOMO. This is also reflected by the extremely low N−N and metal−N stretching frequencies predicted by the calculation (467 and 712 cm^{-1}, respectively; Table 3). The extreme weakening of the N−N bond in **V** is further evidenced by the fact that the σ^* orbital ⟨60⟩ of **V** is at 0.20 au above the SOMO, significantly lowered in energy with respect to that in complex **II** where σ^* was found at 0.26 a.u. above the SOMO.

Single-electron transfer to **V** leads to double occupancy of its HOMO. Upon geometry optimization of the corresponding structure, the N−N bond is cleaved, and the separate components NH_3 and nitrido complex are obtained. It can therefore be concluded that both pathways are in principle effective in the conversion of N_2 to NH_3 on Mo triamidoamine systems, i.e., protolytic cleavage of the hydrazido(2−) complex **IV** and reductive cleavage of the hydrazidium complex **V**. Importantly, both pathways involve an intermediate Mo(IV) hydrazidium species that spontaneously cleaves the N−N bond.

IV. Discussion

In the preceding sections, the mechanism of N−N cleavage in Mo and W hydrazidium complexes with diphos and triamidoamine ligands (diphos = dppe, depe) was evaluated. The N−N splitting process in the Mo/W−NNH_2 and −NNH_3 systems with diphos coligands was investigated on the basis of the dialkylated, doubly reduced, five-coordinate complex [W(dppe)$_2$(NNC_5H_{10})] (compound $\mathbf{B}^W$) a full characterization of which is presented in the accompanying article.[9] As known for the analogous molybdenum complex (compound $\mathbf{B}^{Mo}$), protonation of $\mathbf{B}^W$ in various solvents leads to cleavage of the N−N bond under generation of the nitrido complex and piperidine, providing a prototypical example for the N−N splitting step in the transition-metal-mediated conversion of N_2 to NH_3.

In acetonitrile and at room temperature, compound $\mathbf{B}^W$ reacts much more rapidly with acids than its molybdenum counterpart. A stopped-flow experiment for the reaction of $\mathbf{B}^W$ with $HNEt_3BPh_4$ was therefore performed in propionitrile at −70 °C. As reported in the Results and Analysis section, protonation of $\mathbf{B}^W$ is complete within the dead time of the stopped-flow apparatus, leading to the primary protonated intermediate $\mathbf{B}^WH^+$. Propionitrile coordination to this species proceeds with a rate constant $k_{obs(1)}$ of 1.5 ± 0.4 s^{-1}, generating the intermediate RCN−$\mathbf{B}^WH^+$ (R = Et) that subsequently mediates N−N bond splitting in a slower reaction ($k_{obs(2)}$ = 0.35 ± 0.08 s^{-1}, 6 equiv of acid). A much slower reaction was observed upon treatment of $\mathbf{B}^W$ with $HLutBPh_4$ in benzonitrile at room temperature, proceeding via intermediates that could not be observed in acetonitrile, propionitrile, and THF.

Geometry optimization of a model of the solvent-coordinated, N$_\beta$-protonated intermediate RCN−$\mathbf{B}^WH^+$ was found to spontaneously lead to separation into the nitrido complex and piperidine, corresponding to an activationless heterolytic cleavage of the N−N bond. The much slower N−N cleavage reaction of $\mathbf{B}^W$ in benzonitrile along this pathway was attributed to the delocalization of electronic charge into the aromatic ring of the coordinated solvent molecule. Importantly, DFT also indicates the possibility of activationless N−N cleavage of *unsolvated* intermediate $\mathbf{B}^W$, initiated by protonation at N$_\beta$. In coordinating solvents such as nitriles, this process appears to be intercepted by solvent attack, in agreement with the literature. Nevertheless, this direct reaction path might be relevant to the protolytic N−N cleavage process in non- or weakly coordinating solvents.

For the N−N cleavage reaction of the molybdenum dialkylhydrazido complex $\mathbf{B}^{Mo}$ in acetonitrile, a second, acid-assisted pathway had been observed.[8] This is based on further protonation of RCN−$\mathbf{B}^{Mo}H^+$ at N$_\alpha$ with an equilibrium constant K_3, generating the doubly protonated species RCN−$\mathbf{B}^{Mo}H_2^{2+}$ that subsequently decays to the imido complex and piperidine with a rate constant k_5. The overall rate of this process depends on the product k_5K_3 and thus becomes dependent on the acid concentration. For the protonation of the tungsten complex $\mathbf{B}^W$ in propionitrile at −70 °C, however, no dependence of the reaction rate on the acid concentration could be observed. On the basis of the easier protonability of tungsten as compared to molybdenum NNH_x complexes (x = 0, 1, 2)[21] it was concluded that the equilibrium associated with K_3 is saturated in the presence of an excess of acid. Theoretical simulation of the N−N cleavage process of the doubly protonated intermediate revealed an exothermic process (−45 kcal/mol) with a very small activation barrier (∼1 kcal/mol). Judging from the large value of K_3 for $\mathbf{B}^W$, this must be the dominant pathway for the N−N cleavage reaction of this molecule in the presence of an excess of acid.

In competition with the direct N−N cleavage process triggered by protonation at N$_\beta$, unsolvated $\mathbf{B}^W$ can also be protonated at the metal. As the electron pair in the HOMO of $\mathbf{B}^W$ is consumed for hydride formation, N−N splitting does not occur in this case, even after further protonation at N$_\beta$. Metal protonation therefore would correspond to a nonproductive step in the overall reaction scheme. Judging from the rapid solvent attack on the N$_\beta$-protonated intermediate and from steric considerations, however, this process does not appear to be important. Initial protonation of $\mathbf{B}^W$ at N$_\alpha$, finally, was found to lead to an intermediate that requires

70 kcal/mol to cleave the N−N bond. Nevertheless, N−N cleavage can be induced in this intermediate by transfer of the proton from N_α to N_β, probably via a deprotonation−reprotonation sequence of reactions or by an additional protonation at N_β (cf. Scheme 4).

As a result of the theoretical treatment, protonation of $\mathbf{B}^W$ thus does not allow N−N cleavage (single protonation at N_α), inhibits further protolytic N−N cleavage (protonation at the metal), or induces N−N cleavage as an allowed process (protonation at N_β, along with or without protonation at N_α). This qualitatively agrees with the results of the experimental data available for $\mathbf{B}^W$ and supports the kinetic scheme originally established by Henderson et al.[8] for $\mathbf{B}^{Mo}$ (Scheme 1). So far, the calculations do not indicate the presence of significant activation barriers in the allowed N−N cleavage pathways of $\mathbf{B}^W$ and $\mathbf{B}^{Mo}$. Although activation parameters have not been experimentally determined for this reaction, the fact that the N−N cleavage rate of $\mathbf{B}^W$ becomes slow at low temperature appears to indicate the presence of a barrier in this process. Possibly, our theoretical picture of initial proton transfer to compound **B** is too simple, and the primary interaction of the acid with compound **B** is more in the form of an H-bonded acid−base complex.[25] In this complex, the actual proton transfer might occur only after elongation of the N−N bond, i.e., concomitant with the N−N cleavage process, introducing a barrier along the N−N coordinate.

Solvent coordination to the primary protonated intermediate $\mathbf{B}H^+$ appears to be associated with a barrier as well. The fact that nitrile does not coordinate to the starting complex has already been noted by Henderson et al.[8] The reason for this finding is the lone pair at the metal pointing into the vacant site. Compound **B** thus is not Lewis acidic but rather *Lewis basic* and will not easily accept a solvent. Coordination of nitriles to the monoprotonated form is slow because this intermediate does not bend at N_α after initial protonation and thus still has a lone pair at the metal. This only changes upon bending of $\mathbf{B}H^+$ at N_α, thus giving a Lewis acidic character to this species and allowing coordination of solvent. Moreover, bending is associated with an orbital redistribution, shifting two electrons from a dσ- to a dπ-type metal orbital. Solvent coordination to $\mathbf{B}H^+$, therefore, is associated with an activation barrier; the calculation gives +16 kcal/mol. In particular, it becomes slower at low temperatures than observed in the room-temperature experiment of Henderson et al.[8] where it was complete within the dead time of the stopped-flow apparatus. Alternatively, initial protonation at N_α or initial double protonation at N_α and N_β should lead to an intermediate that is bent at N_α and thus readily would accept a solvent molecule. Judging from the slow solvent coordination observed for $\mathbf{B}^W$ at low temperature, these scenarios appear less probable.

In the second part of this article, a theoretical analysis of the reduction and protonation of N_2 in the Mo(III) triamidoamine system up to the point of N−N cleavage and generation of the first molecule of NH_3 is presented. To this end, DFT calculations of the $Mo^{III}N_2$ complex and its diprotonated, one-electron-reduced NNH_2 derivative **II** were performed. Calculated structural and spectroscopic parameters were compared to available experimental data. Moreover, the postulated one-electron-reduced derivative of **II**, intermediate **III**, was treated by DFT. For the cleavage of the N−N bond, two scenarios were considered: (i) one-electron reduction of the Mo^V-NNH_2 complex **III** leading to a $Mo^{IV}-NNH_2$ complex, followed by protonation, and (ii) protonation of the Mo^V-NNH_2 complex **III** to a Mo^V-NNH_3 species, followed by one-electron reduction. In both cases, geometry optimization of the intermediate Mo(IV) hydrazidium species leads to the separated nitrido complex and ammonia; i.e., both reaction modes mediate a spontaneous N−N cleavage process. Judging from the lower-lying LUMO for **V** as compared to **III**, pathway ii appears more favorable than pathway i; i.e., protonation of the NNH_2 group of **III** to a hydrazidium species before electron transfer to induce N−N cleavage helps to make the necessary reduction potential less negative. On the other hand, the terminal NH_2 group of **III** is still slightly positive (+0.11), in contrast to that of its one-electron-reduced counterpart **IV** (−0.05, cf. Table 3). Therefore, **IV** is easier to protonate than **III**. The actual pathway will thus depend on the applied reduction potential and the pK_a value of the acid effective in the protonation.

What are the implications of the geometric and electronic structures on the reactivities of the Mo/W diphos and the Mo triamidoamine systems? Most notably, the diphos systems bind dinitrogen at the zerovalent stage (d^6 configuration), whereas N_2 binding of the triamidoamine ligands occurs at the Mo(III) level. Judging from N−N distances, N−N stretching frequencies, and calculated charges, the activation of N_2 is comparable in both systems. Importantly, the three negatively charged equatorial amido groups in the trigonal triamidoamine system are both strong σ and strong π donors, pushing the $d_{xy}/d_{x^2-y^2}$ orbitals to high energy by σ/π-antibonding interactions such that they become unoccupied. Thus, only the amide nonbonding d_{xz} and d_{yz} orbitals are populated and interact with the dinitrogen π^* orbitals. In contrast, the neutral, equatorial phosphine groups of the Mo/W diphos systems are σ donors and π acceptors, generating (along with the axial ligands) a set of two d_σ orbitals and a set of three d_π orbitals. At the zerovalent level of the metal center, the d_π orbitals are occupied by six electrons. However, whereas the two electrons in the nonbonding d_{xy} orbital are not involved in the reduction of N_2 to NH_3 on Mo(0) or W(0) complexes at any stage, all three metal d_π electrons are needed for this process in the Mo triamidoamine system. The latter system therefore is more economical in the use of reduction equivalents.

A second important difference between the two systems relates to fact that the ligand in the trans position to the N_2 coordination site is fixed in the triamidoamine complex. In contrast, this ligand is exchangeable in Mo/W diphos complexes and lost upon two-electron reduction at the NNH_2 and NNR_2 stage, forming five-coordinate species. However, a solvent molecule or the conjugate base of the employed acid can coordinate to the empty coordination site just after

(25) Golubev, N. S.; Shenderovich, I. G.; Smirnov, S. N.; Denisov, G. S.; Limbach, H.-H. *Chem.—Eur. J.* **1999**, *5*, 492.

protonation of the reduced intermediate, re-forming a six-coordinate complex. *The actual N−N cleavage process of this solvent-coordinated intermediate is entirely analogous to that described for the triamidoamine system.* In both cases, the reactive species—a Mo(IV)/W(IV) complex in that and a Mo(II) complex in the diphos system—exhibits a hydrazidium group which is bent at N_α, forming a lone pair at this position. The HOMO of this intermediate is an in-plane metal d_π orbital with an antibonding contribution of the lone pair at N_α. Moreover, it contains a p-orbital at N_β that is directed along the N−N bond and is antibonding with respect to the lone pair at N_α. Upon N−N cleavage, this HOMO evolves to the lone pair of ammonia, and the two-electron-oxidized metal nitrido species is left behind.

Acknowledgment. The authors gratefully acknowledge financial support from Deutsche Forschungsgemeinschaft (SFB 583 and TU58/12-1) and Fonds der Chemischen Industrie.

Supporting Information Available: Charge contributions of models **II** and **IV**; UV/vis absorption spectra of compound $\mathbf{B}^{W}$ in propionitrile (with and without acid) and in benzonitrile (with acid); UV/vis absorption spectrum of $[W(N)(NCPh)(dppe)_2]BPh_4$ in benzonitrile; ^{15}N NMR spectra of compound $\mathbf{B}^{W}$ in benzonitrile, with and without acid; PES for the N−N cleavage reaction of the α-protonated intermediate. This material is available free of charge via the Internet at http://pubs.acs.org.

IC048674O